THE JOURNAL OF PHYSICAL CHEMISTRY LETTERS
A JOURNAL OF THE AMERICAN CHEMICAL SOCIETY

pubs.acs.org/JPCL Letter

Anomalous Dependence of Photocarrier Recombination Time on the Polaron Density of TiO_2(110)

Huimin Wang, Huixia Fu, Peiwei You, Cui Zhang, Ying Jiang,* and Sheng Meng*

Cite This: *J. Phys. Chem. Lett.* 2023, 14, 8312−8319 Read Online

ACCESS | Metrics & More | Article Recommendations | Supporting Information

ABSTRACT: Polarons play a crucial role in energy conversion, but the microscopic mechanism remains unclear since they are susceptible to local atomic structures. Here, by employing *ab initio* nonadiabatic dynamic simulations, we investigate electron−hole (e-h) nonradiative recombination at the rutile TiO_2(110) surface with varied amounts of oxygen vacancies (V_o). The isolated V_o facilitates e-h recombination through forming polarons compared to that in the defect-free surface. However, aggregated V_o forming clusters induce an order-of-magnitude acceleration of polaron diffusion by enhancing phonon excitations, which blocks the defect-mediated recombination and thus prolongs the photocarrier lifetime. We find that photoelectrons are driven to migrate toward the top surface due to polaron formation. Our results show the many-body effects of defects and polaron effects on determining the overall recombination rate, which has been ignored in the Shockley-Read-Hall model. The findings explain the controversial experimental observations and suggest that engineering V_o aggregation would instead improve photocatalysis efficiencies in polaronic materials.

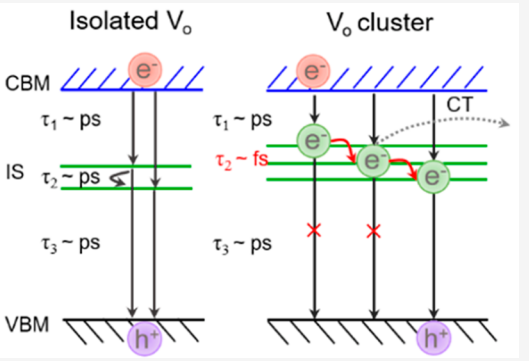

Polarons, i.e., the quasiparticles composed of excess carriers dressed with virtual phonons, play a critical role in multiple physicochemical properties of materials, including superconductivity, ferroelectricity, and photocatalysis.[1−8] Point defects facilitate polaron formation by introducing unpaired electrons/holes. Taking the most studied photocatalyst, the rutile TiO_2(110) surface, as an example,[9] oxygen vacancies (V_o) introduce small polarons in their surroundings, which lead to localized electronic states in the band gap, extending surface photoactivity to the visible-light region.[10−13] Manipulating characteristics of V_o (e.g., concentrations and distributions) concurrently changes the polaron configurations, which influence the adsorption strength and decomposition rate of molecules,[14,15] or drive surface reconstructions.[16] The strong correlation between defects and polarons provides unique pathways for controlling the properties of quantum materials by engineering defects.[17−20] Although well studied in the thermal equilibrium regime, polaron effects on nonequilibrium carrier dynamics are underexplored since they are sensitive to local atomic structures,[21] and thus the detection challenges the state-of-the-art experimental techniques, requiring both ultrafast time resolution and atomic spatial resolution.

To achieve high efficiency in optoelectronic devices, nonradiative e-h recombination, which converts electronic energy into heat, should be greatly suppressed. Point defects generally facilitate nonradiative recombination by capturing electrons/holes. The Shockley-Read-Hall (SRH) statistic model is widely used to estimate the rate of defect-mediated recombination based on the density and energy level of defect states only.[22] It predicts that defect states with energy levels closer to the midbandgap (i.e., deeper defects) have a higher recombination efficiency and assumes that the total recombination rate increases linearly with the defect density.

The presence of V_o in metal oxides triggers various chemical reactions[23−27] but may also damage photocarrier lifetime and mobility. Therefore, unravelling the role of V_o with different characteristics in nonradiative recombination is critical for improving photocatalytic efficiency. Previous first-principles studies confirmed that single V_o on the TiO_2(110) surface serves as an effective SRH recombination center by introducing the deep polaronic in-gap states.[28] However, the structure model is too simple to capture realistic conditions. Theoretical prediction contradicts the quantitative experimental measurements, which show that the photocarrier lifetime is prolonged instead on the TiO_2(110) surface with a higher concentration of V_o.[29] Similarity, the anomalous increase in the photocarrier lifetime as the V_o density rises is found in tungsten trioxide (WO_3) as well, where the polaronic effects are strong.[30] These experimental results suggest that in polaronic materials, the dependence of e-h recombination

Received: June 20, 2023
Accepted: August 29, 2023
Published: September 8, 2023

https://doi.org/10.1021/acs.jpclett.3c01685
J. Phys. Chem. Lett. 2023, 14, 8312−8319

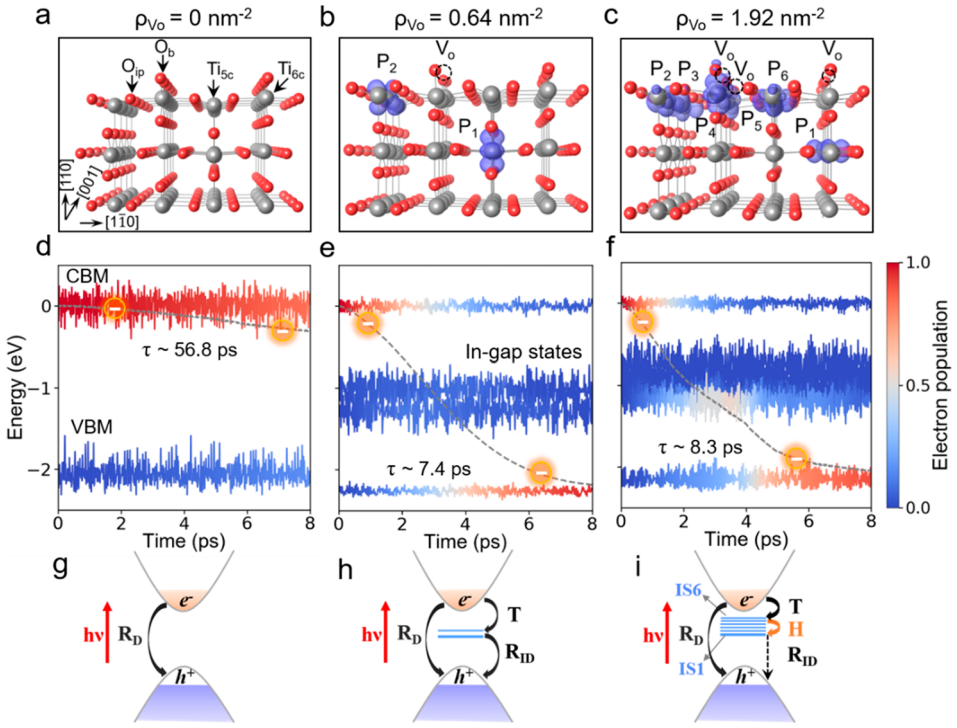

Figure 1. Ground state properties and time dependent e-h recombination dynamics on the TiO_2(110) surface with different V_o densities. (a–c) Optimized atomic structures of the surface with ρ_{Vo} = 0, 0.64 and 1.92 nm^{-2}, respectively. The top surface is composed of the hexacoordinated Ti (Ti_{6c}), pentacoordinated Ti (Ti_{5c}), in-plane oxygen (O_{ip}), and bridge oxygen (O_b). The dashed circle denotes the position of V_o. The charge density distributions of polarons are shown by purple areas with an isosurface of 0.03 e/Å^3 and counted from low to high energy level. (d–f) Time evolution of KS eigenvalues and electron population on frontier orbitals. The KS eigenvalues of the CBM, VBM, and in-gap states oscillate with time due to electron–phonon scatterings. The gray dashed lines show the energy decay of the photoexcited electrons. The e-h recombination time τ is labeled. (g–i) Schematics of different recombination pathways on the three surfaces with different ρ_{Vo}. The pathways include direct recombination (R_D), polaron formation by photoelectron self-trapping (T, with time τ_1), polaron diffusion between in-gap states (H, with time τ_2), and indirect recombination between polarons and holes (R_{ID}, with time τ_3).

time on the defect density deviates from the prediction of the SRH model, while the underlying mechanism at the molecular scale remains elusive. Although the recombination efficiency of single defect can be accurately estimated based on an extended SRH model[31] or first-principles techniques,[32−36] these theoretical works rarely take the interactions of multiple defects into consideration, which would show a great importance on the overall recombination rate by affecting correlated polaron dynamics.

Here, we investigate e-h recombination dynamics on the rutile TiO_2(110) surface with various V_o distributions via time-domain first-principles nonadiabatic molecular dynamics (NAMD) simulations.[37,38] We find that e-h recombination time first decreases but then slightly increases with increasing local V_o density (ρ_{Vo}), not fully obeying the SRH model but consistent with experimental observations. When V_o dispersedly distributes on the surface with ρ_{Vo} < 0.64 nm^{-2} (an estimated value corresponds to a single V_o on the (4 × 2) supercell), photoexcited electrons quickly recombine with holes by forming polarons compared to that in the defect-free region. However, when multiple V_o assemble with ρ_{Vo} > 0.64 nm^{-2}, enhanced electron–phonon interactions (EPI) induce an order-of-magnitude acceleration of polaron diffusion. As a result, trapped photoelectrons tend to rapidly diffuse among different polaron configurations instead of recombining until they reach the most stable one, and the remaining recombination pathway slows simultaneously, thus prolonging photocarrier lifetime. We find that polaron formation induces photoelectrons to migrate toward the top surface before recombination, and the migration rate is accelerated by increasing ρ_{Vo}. Our results reveal the high sensitivity of nonequilibrium polaron dynamics to local atomic structures, which modulates photocarrier recombination microscopically. The large photocarrier lifetime and accelerated charge migration promise improvements in photocatalytic efficiencies when V_o aggregates at the oxide surface.

Figure 1 depicts the atomic structures and e-h recombination dynamics on the rutile TiO_2(110) surface with three different V_o concentrations. The absence of a bridge oxygen atom (V_o) on the 4 × 2 slab of the TiO_2(110) surface introduces two small polarons, which are self-trapped at neighboring Ti sites, inducing in-gap states at ∼1.1 eV below the conduction band minimum (CBM, see Supporting Information Figure S1). There exist multiple polaron configurations within the energy difference of ∼0.3 eV.[11,17,19,39,40] Polarons mostly stay in the subsurface under Ti_{5c} atoms and occasionally hop to the top surface, especially at the Ti_{5c} atoms.[11,39] The dynamic behaviors of polarons are prominent at room temperature. We confirm that different polaron configurations with the same V_o concentration, which are clearly observed or indicated in experiments, slightly modify the position of in-gap states as well as the photoexcited dynamics (Figure S2).

https://doi.org/10.1021/acs.jpclett.3c01685
J. Phys. Chem. Lett. 2023, 14, 8312−8319

When ρ_{Vo} is increased from 0.64 nm^{-2} (Figure 1b) to 1.92 nm^{-2} (i.e., three V_o on the surface slab, Figure 1c), the amount of polarons in the nano-region of surface increases simultaneously. Meanwhile, a higher proportion of polarons is distributed at the top surface, and in-gap states have energy levels closer to the CBM and a narrower band gap between them (see Figure S1), which are the competition results of many-body interactions among polarons, i.e., repulsive interactions between polarons and attractive interactions between polarons and V_o.[19] Here we simulate the locally high concentration of V_o instead of the global behavior of the TiO_2(110) surface.

Upon the above band gap excitation (both valence electrons and V_o-derived polarons are excited), e-h pairs are generated and relax to the band edge in hundreds of femtoseconds with a time scale comparable for the three cases (Figure S3). Afterward, most of e-h pairs are nonradiatively recombined due to electron−phonon scatterings by pathways including (i) direct recombination (R_D), i.e., photoelectrons directly transition from the CBM to the valence band maximum (VBM); (ii) indirect pathways on the defective surfaces with three subprocesses: photoelectrons are trapped by in-gap states (T process) first and/or diffuse to other in-gap states (H process), and then recombine with holes (R_{ID} process) (see schematics in Figure 1(g−i)). The overall nonradiative e-h recombination is the result of competition among these pathways.

The time evolution of electron population on each frontier orbital (including the CBM, VBM, and in-gap states) is shown in Figure 1(d−f) for the three cases. A linear fit to the increase in electron population on the VBM is used to estimate the e-h recombination time (i.e., photocarrier lifetime τ). When V_o exist, the photocarrier lifetime is reduced greatly in comparison to that in the defect-free surface (τ = 56.8 ps for the defect-free case where ρ_{Vo} = 0 nm^{-2}); however, it is counterintuitively shorter on the surface with isolated V_o (τ = 7.4 ps for ρ_{Vo} = 0.64 nm^{-2} with configuration 1 and τ = 6.0 ps with configuration 2) than that with multiple V_o (τ = 8.3 ps for ρ_{Vo} = 1.92 nm^{-2}). Besides, ∼50% of photoelectrons are self-trapped at the lowest in-gap state (IS1) at 3.4 ps on the surface with dense V_o (Figure 1f), whereas that is always less than 10% on the surface with sparse V_o (Figure 1e), indicating that polaron dynamics is strongly influenced by the local V_o concentration.

To explain the nonmonotonic dependence of photocarrier lifetime on defect density, we divide the recombination process into two substages, and the role of in-gap states at each stage is revealed. In the initial stage of recombination (t = 0−50 fs), direct e-h recombination (R_D) and photoelectron self-trapping (T) occur, contributing to an increase in the electron population on the VBM and in-gap states, respectively. Taking a moment at this stage, for example (e.g., t = 50 fs, see Figure 2(a)), the rate of R_D is marginally influenced by varied ρ_{Vo}, while the T process is accelerated obviously as ρ_{Vo} grows, indicating that a larger percentage of photoelectrons form polarons before recombination when more V_o aggregates on the surface. The dependence of polaron formation time (τ_1, see Figure S4) on V_o density agrees well with previous experimental findings,[21] i.e., the retrapping of polarons upon visible-light excitation occurs faster in the nano-region with more V_o, and our results additionally provide the microscopic explanation.

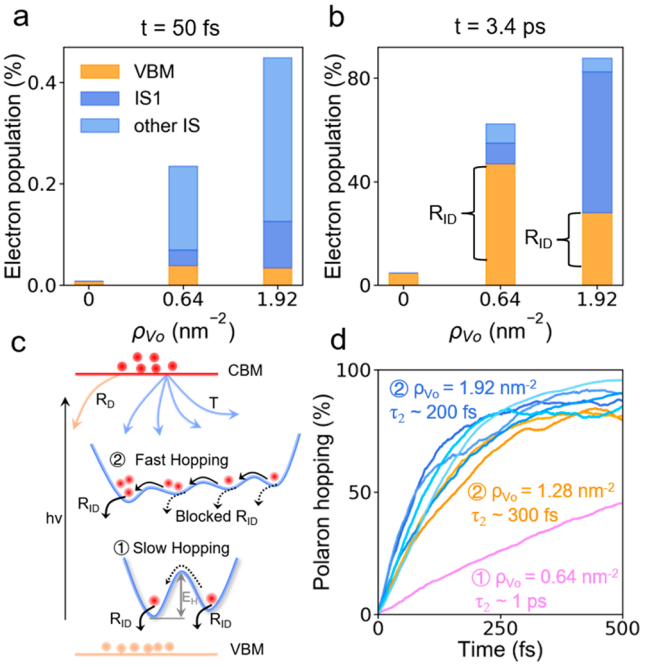

Figure 2. Influence of polaron diffusion on e-h recombination. (a, b) Transient electron population on the VBM and in-gap states at t = 50 fs and t = 3.4 ps, respectively. In the second stage, the proportion of indirect recombination is labeled. (c) Schematics of two different recombination mechanisms. The energy barrier of polaron hopping is labeled as E_H. (d) The rate of polaron hopping on the surface with ρ_{Vo} = 0.64, 1.28, and 1.92 nm^{-2}. The vertical axis shows electron population on the lower in-gap state when polarons hop between two adjacent in-gap states. The multiple pathways for polaron diffusion on the surface with ρ_{Vo} = 1.92 nm^{-2} (1.28 nm^{-2}) are represented by different shades of blue (orange) lines. The polaron hopping time τ_2 is labeled.

In the second stage (t > 50 fs), polaron diffusion (H) and indirect recombination (R_{ID}) occur, changing electron population between the VBM and in-gap states. Using t = 3.4 ps for quantitative analysis (see Figure 2b), although the number of relaxed photoelectrons is largest on the surface with the highest ρ_{Vo} (1.92 nm^{-2}), fewer of them are recombined in comparison to those on the surface with low ρ_{Vo} (0.64 nm^{-2}). Instead, most of polarons diffuse to the lowest in-gap states (IS1) on the highly reduced surface. As ρ_{Vo} rises, the recombination between polarons and holes slows anomalously, which prolongs the photocarrier lifetime and reduces energy dissipation from the electron to phonon subsystems.

The alteration of the e-h recombination mechanism with increasing ρ_{Vo} can be understood by the change of nonadiabatic coupling (NAC), which controls interband transition rate in the NAMD frameworks (see Methods). The NAC element is defined as

$$d_{jk} = \sum_I -i\hbar \frac{\langle \widetilde{\phi_j} | \nabla_{R_I} \mathcal{H} | \widetilde{\phi_k} \rangle}{\varepsilon_k - \varepsilon_j} \cdot \dot{R}_I \quad (1)$$

where $\mathcal{H}$ is the Hamiltonian; $\widetilde{\phi_j}(\widetilde{\phi_k})$ and $\varepsilon_j(\varepsilon_k)$ are the wave function and eigenvalue of the KS state j (k); R_I is the coordinate of the Ith atom. The NAC is proportional to nucleus velocity $\dot{R}_I$ and electron−phonon coupling (EPC) strength $\langle \widetilde{\phi_j} | \nabla_{R_I} \mathcal{H} | \widetilde{\phi_k} \rangle$, but is inversely proportional to the

https://doi.org/10.1021/acs.jpclett.3c01685
J. Phys. Chem. Lett. 2023, 14, 8312−8319

energy level difference $\varepsilon_k - \varepsilon_j$. The average NAC matrix along the MD trajectory between frontier orbitals is shown in Figure 3(a–c). The negligible change in NAC between the CBM and VBM explains the minor variation in the R_D rate as ρ_{Vo} increases (Figure 2a). The case is similar for the individual T path, and thus the overall efficiency of polaron formation is mainly determined by the density of empty in-gap states (Figure S4). In contrast, NAC between adjacent in-gap states is obviously enhanced with ρ_{Vo} increasing from 0.64 to 1.92 nm^{-2}, which lowers the energy barrier of polaron hopping,[41] resulting in an order of magnitude acceleration of polaron diffusion (Figure 2d). In addition, we find that NAC between the IS1 and the VBM is weakened due to the enlarged energy gap with increasing ρ_{Vo} (Figure S6).

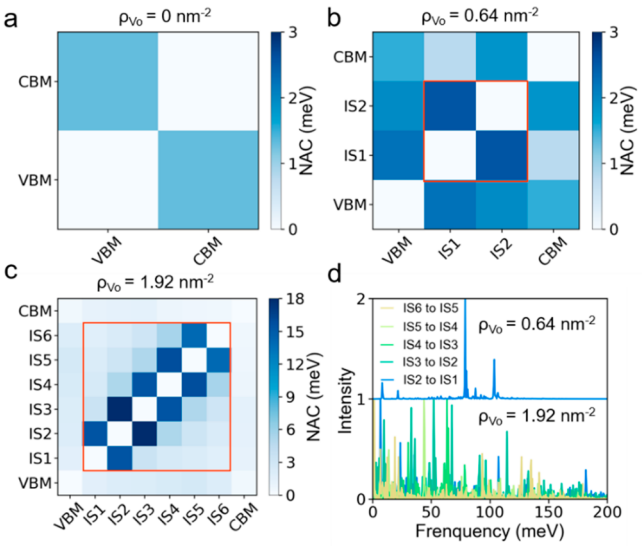

Figure 3. (a–c) NAC matrix between frontier orbitals on the surface with different ρ_{Vo}. The red box highlights the NAC between in-gap states. (d) Phonon modes coupled to polaron diffusion between adjacent in-gap states. The intensities of phonon modes are normalized on the two surfaces individually and shifted vertically for clarity.

The analysis of NAC is rationalized by the phonon excitations that contribute to the interband transition of carriers (see Methods). As ρ_{Vo} rises, more atomic vibrations assist polaron diffusion, shown by the enhanced vibrational intensity and broadened vibrational frequency (Figure 3d). It indicates that varying V_o density in nano-region influences phonon excitation, which has a strong impact on the polaron hopping rate. Meanwhile, phonon modes coupled to electron transition from the CBM to the highest in-gap state are slightly reduced with increasing ρ_{Vo} (see Figure S5(a–b)), leading to slower charge trapping along this pathway. These effects cocontribute to the prolonged photocarrier lifetime when more V_o assemble on the surface.

Based on the above analysis, two recombination scenarios are proposed and distinguished by the relative rate of polaron diffusion (H) and polaron-mediated recombination (R_{ID}, see schematics in Figure 2c). In general, R_{ID} is achieved in several picoseconds (Figure S6). The time scale of polaron hopping under thermal equilibrium was estimated to be ∼4.5 ps at 100 K and ∼0.42 ps at 700 K.[17] Upon photoexcitation, excess electrons are pumped to the conduction bands within femtoseconds, leaving polaronic lattice distortions that do not relax back to the undistorted structures. Afterward, photoelectrons rapidly diffuse between empty in-gap states without the migration of lattice distortions, i.e., obeying the nonadiabatic polaron hopping picture. Polaron transport under nonequilibrium is slightly faster than that under thermal equilibrium condition but still remains ∼1 ps when ρ_{Vo} = 0.64 nm^{-2}. It is obviously accelerated to ∼200 (300) fs when ρ_{Vo} increases to 1.92 (1.28) nm^{-2} (Figure 2d).

When the rate of H and R_{ID} is comparable (i.e., "slow hopping regime"), each polaron-mediated recombination channel is feasible, and thus the overall recombination time continuously reduces with increasing ρ_{Vo}. However, when H becomes an order of magnitude faster than R_{ID} (i.e., "fast hopping regime"), rapid polaron diffusion prevents e-h recombination, until photoelectrons transfer to the most stable configuration (IS1), which explains the prominent increase in electron population on IS1 (Figure 1f). The recombination between nonequilibrium polaron states and holes may occur, but with a low probability. When photoelectrons occupy the most stable polaron sites, they could hop to other possible

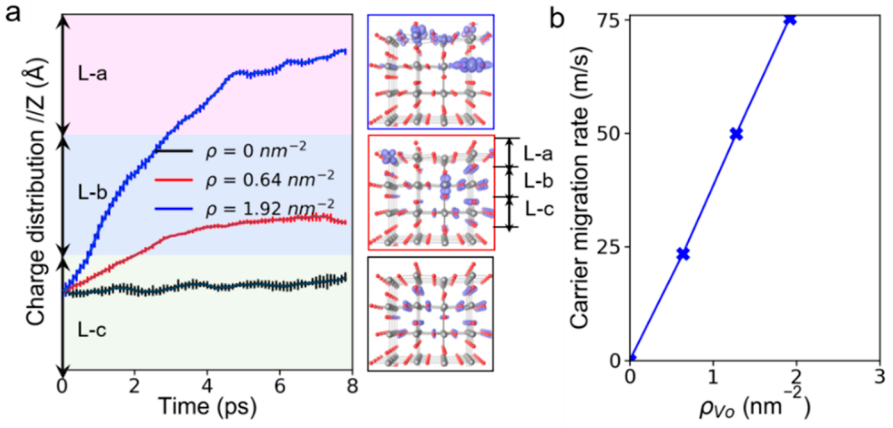

Figure 4. (a) Time evolution of the average coordinate of photoelectrons projected along the [110] direction (z axis) during e-h recombination. The error bars are added by sampling 100 MD trajectories. The right panels show the charge density distributions of photoelectrons at 3 ps. The first, second, and third layer of the surface are labeled as L-a, L-b, and L-c, respectively. The isosurface charge density is 0.03 e/Å^3 (0.006 e/Å^3) on defective (defect-free) surfaces. (b) The migration rate of photoelectrons along the z axis as a function of ρ_{Vo}.

https://doi.org/10.1021/acs.jpclett.3c01685
J. Phys. Chem. Lett. 2023, 14, 8312–8319

sites, but recombination is more energetically favorable. Therefore, in this concentration range, R_{ID} through high energy-level in-gap states (i.e., IS2 to IS6) are nearly blocked because of the competition between fast polaron hopping and slow recombination, and the remaining R_{ID} channel by IS1 slows down simultaneously (Figure S6), eventually leading to an increase in photocarrier lifetime.

The influence of polaron diffusion on e-h recombination is confirmed on the surface with moderate ρ_{Vo} (1.28 nm^{-2}), where polaron diffusion also occurs in hundreds of femtoseconds, blocking most of indirect recombination pathways (Figure 2d and Figure S7). Furthermore, we confirm that the space distributions of V_o with the same density have a minor effect on the polaron diffusion rate due to similar phonon excitation (Figure S8), thus leading to the comparable photocarrier lifetime.

Apart from the time evolution of nonequilibrium electron population, we also monitor the real-space trajectory of photoelectrons. The average coordinate of photoelectrons is defined as $\boldsymbol{r}(t) = \sum_i C_i(t) \langle\varphi_i(t)|\hat{\boldsymbol{r}}|\varphi_i(t)\rangle$ (2), where $C_i(t)$-$(\varphi_i(t))$ is the time-evolved electron population (wave function) of KS state *i*. The projection of electron coordinates along the [110] direction (*z* axis) is shown in the left panel of Figure 4a. Upon photoexcitation, e-h pairs are generated in the deep layer of the TiO_2(110) surface (i.e., L-c layer). Then, photoelectrons are driven to migrate toward the upper layer of surface due to carrier self-trapping around V_o, while they remain at the interior on the defect-free surface until recombination. The right panels of Figure 4a show the charge density distributions of photoexcited electrons at 3 ps. It is clear that ∼50% of photoelectrons are distributed at the first layer (i.e., L-a layer) of the surface with the highest ρ_{Vo} = 1.92 nm^{-2}, while most of them remain at the second layer and the third layer of the surface with ρ_{Vo} = 0.64 and 0 nm^{-2}. A proportion of photoelectrons are trapped at in-gap states, forming polarons on the surface and the subsurface, and the rest occupy the CBM and delocalize at the deep sub-subsurface when ρ_{Vo} = 1.92 nm^{-2}. The migration rate of photoelectrons along the *z* axis increases linearly with ρ_{Vo} (Figure 4b), indicating that increasing the V_o density can improve the efficiency of charge transfer (CT) to surface adsorbates.

Figure 5a presents the phase diagram of photocarrier lifetime as a function of ρ_{Vo}, which is separated into two regions at a critical density (ρ'_{Vo} = 0.64 nm^{-2}). Below ρ'_{Vo}, the photocarrier lifetime decreases with increasing ρ_{Vo}, due to the proportional increase of recombination channels (left panel in Figure 5b). Above the threshold, polaron diffusion within hundreds of femtoseconds leads to the closure of indirect recombination pathways and the anomalous increase in the photocarrier lifetime, which deviates from the prediction of the SRH model, i.e., photocarrier lifetime is inversely proportional to the defect density (right panel in Figure 5b). Different from the global increase in V_o density to drive the surface reconstruction,[16] here we investigate atomic-scale distributions of defects in the sub-nanometer region. The local aggregation of two or three V_o forming clusters does not induce global phase transition but has a strong impact on the polaron diffusion rate.

Our findings are supported by available experimental results. First, the estimated photocarrier lifetime is quantitatively consistent with that measured by Ozawa et al., which had eliminated the influence of the surface band bending and provided an intrinsic carrier lifetime on the slightly reduced

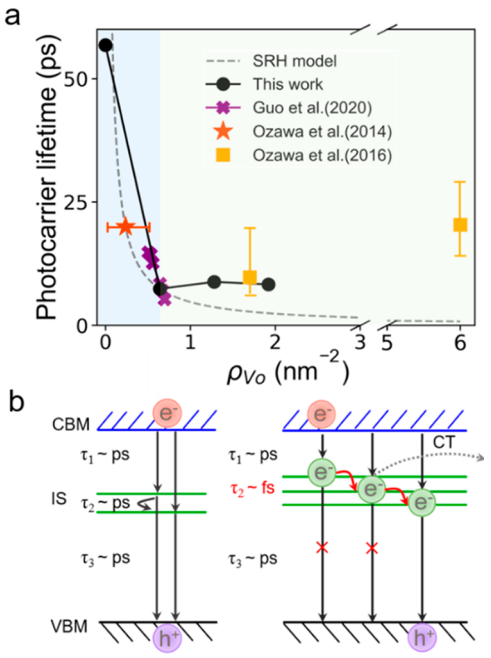

Figure 5. (a) Phase diagram of photocarrier lifetime as a function of ρ_{Vo}. The red star, purple line, and orange squares show experiments data of the photocarrier lifetime obtained in ref 43, ref 21, and ref 29. Due to the temperature difference between experiments (T = 10 K) and first-principles simulations (T = 100 K), the data in ref 21 is uniformly scaled by 6×10^{-6}, which corresponds to an energy barrier $E_a \approx 11$ meV as the recombination probability $r \propto \exp\left(\frac{-E_a}{k_B T}\right)$, where k_B is the Boltzmann constant.[43] Since the surface photovoltage effect prolongs the detected photocarrier lifetime in experiments, the data in ref 29 are uniformly scaled by 8.8×10^{-5}, which indicates the surface energy barrier $E_b \approx 240$ meV as $r \propto \exp\left(\frac{-E_b}{k_B T}\right)$. The gray dashed line shows the tendency predicted by the SRH model,[31,35] i.e.,$\tau = \frac{1}{\rho_{Vo}{}^* R}$, where R is the recombination efficiency of single defect. (b) Two recombination mechanisms involving slow (left) and fast (right) polaron diffusion. The time scales of photocarrier self-trapping (τ_1), polaron hopping (τ_2), and indirect recombination (τ_3) are labeled.

TiO_2(110) surface.[42] The consistency between simulations and experiments demonstrates the accuracy of our theoretical framework (see Methods). Second, in this concentration region, the relation of photocarrier lifetime with ρ_{Vo} shows good agreement with that measured by Guo et al. after the uniform data rescaling.[21] Third, Ozawa et al. reported that e-h recombination is delayed on the (1 × 1) phase of TiO_2 (110) as ρ_{Vo} grows above the threshold, and attributed it to a macroscopic effect, i.e., the enhancement of surface photovoltage,[29] while the underlying microscopic mechanism remains elusive until the analyses in the present work.

At present, the determination of polaron configurations on the rutile TiO_2(110) is still an open question. The prevailing views are that there are multiple polaron configurations with similar energy scales.[11,19,39,40,44] Among them, the most stable one is two polarons located at the subsurface. The polaron configuration of one at the subsurface and another at the surface Ti_{5c} is more stable than the rest of the configurations. The dynamic behaviors of polarons indicated in experiments have been confirmed by ab initio MD simulations adopting different set-ups.[11,19,39,40,44] We demonstrate that the e-h

https://doi.org/10.1021/acs.jpclett.3c01685
J. Phys. Chem. Lett. 2023, 14, 8312−8319

recombination time is slightly influenced by different polaron configurations but is closely related with the polaron density (Figures S2 and S7). Due to the polaronic nature, it is difficult to detect polarons with high formation energy by scanning tunneling microscopy (STM) at an ultralow temperature.

The temperature effect on e-h recombination at the TiO_2(110) surface with different ρ_{Vo} values is also investigated. It is demonstrated that elevating temperature (from 100 to 300 and 500 K) obviously reduces the photocarrier lifetime on the defect-free surface, whereas it only slightly changes that on the defective surfaces with V_o (Figures S9−10). The suppressed temperature effect is related to the reduced energy barrier (E_a) by introducing polaronic in-gap states. Meanwhile, e-h recombination kinetics show that as the temperature increases, all recombination channels are accelerated due to the enhanced thermal phonon excitation, while the acceleration of polaron diffusion is particularly dominant, resulting in more frequent polaron diffusion before recombination on the defective surfaces.

The important role of polaron dynamics in e-h recombination can be extended to other quantum materials and help us to understand their exotic photoexcitation dynamics. For example, the wavelength-dependent photoconversion efficiency in hematite (α-Fe_2O_3) is inferred to be concerned with the light-modulated polaron formation and hopping rate, by fitting experimental data with empirical models.[45] Our results give a clear microscopic explanation to their speculation. Polaron hopping can be accelerated under certain photoexcitation conditions by promoting specific lattice vibrations, which prevents indirect e-h recombination and improves the photocarrier lifetime and mobility. Besides, the anomalous slowdown of photoelectron relaxation with increasing V_o in WO_3 films[30] may provide an experimental support for the present results. Due to the lack of evidence to illuminate the underlying mechanism, the role of V_o in photocarrier recombination is still obscure. Here we propose a rational microscopic picture considering the V_o-derived polaron effects under nonequilibrium based on the time-domain NAMD simulations. We admit that other physiochemical properties in WO_3 (e.g., ferroelectricity or surface polarization) related to polaron effects would complicate the microscopic processes, which require high-resolution experiments to decipher them in the future.

Our results explicitly reveal that in polaronic materials, the interactions between multiple defects play a critical role in determining the overall nonradiative recombination rate, which has been ignored in the SRH model and previous first-principles investigations, where only the recombination efficiency of single defect is considered.[31,33−36] Due to the many-body effects of defects and related nonequilibrium polaron dynamics, although the single defects serve as an effective recombination center, forming V_o clusters would prolong the photocarrier lifetime and promote charge transfer. Since polaron transfer is sensitive to phonon excitations, its rate can be modulated by varying the defect concentration or applying external fields. For example, the aggregation of multiple V_o can be observed and controlled by STM,[17] which provides a pathway for manipulating the photocarrier lifetime. In contrast, photoelectrons captured by "deep" defects without polaron effects are difficult to detrap and diffuse in the real space, and thus the photocarrier lifetime always decreases with increasing defect concentrations.[35]

In conclusion, we demonstrate that due to the defect-derived polaron effects, nonradiative electron−hole recombination time depends non-monotonically on local V_o density at the rutile TiO_2(110) surface, extending the SRH model by considering interactions between defects. When V_o distribute sparsely ($\rho_{Vo} < 0.64$ nm^{-2}), polaron formation facilitates e-h recombination, leading to a continuous decrease in the photocarrier lifetime with increasing ρ_{Vo}. However, when V_o aggregate forming complexes ($\rho_{Vo} > 0.64$ nm^{-2}), polaron diffusion is accelerated by an order of magnitude due to enhanced phonon excitation. When it becomes an order of magnitude faster than e-h recombination, photoelectrons diffuse between in-gap states before relaxing to the valence bands. The many-body effects of polarons induce the reduction of indirect recombination pathways as well as the recombination efficiency by a single polaron state, thus prolonging the photocarrier lifetime. Besides, polaron formation induces photoelectrons to migrate from deep to shallow surface sites, and the migration rate accelerates with increasing ρ_{Vo}. Our results show the critical role of nonequilibrium polaron dynamics in photocarrier recombination. Since the existence of V_o is a double-edged sword for photoelectrochemical reactions, our findings suggest that controlling V_o local aggregation, instead of dispersion, on the TiO_2(110) surface would improve the performance of photocatalysis by promoting photoelectron migration without deteriorating their lifetime.

METHODS

The *ab initio* nonadiabatic molecular dynamics (NAMD) are performed based on the mixed quantum-classical fewest switched surface hopping (FSSH) method implemented within the time-dependent Kohn−Sham (TDKS) density functional theory[46] (Note S1). The classical pathway approximation is adopted in our computational framework; i.e., ionic dynamics are beforehand evolved along adiabatic PES with a ground-state electronic structure, and then carrier relaxation is simulated based on the nonadiabatic couplings (NAC) between KS orbitals.

The static and *ab initio* molecular dynamic (AIMD) calculations are performed based on the spin-polarized and Hubbard-corrected density functional theory (DFT+U) as implemented in the Vienna *ab initio* simulation package (VASP).[47] The Perdew-Burke-Ernzerholf (PBE)[48,49] exchange-correlation functionals and projector-augmented wave (PAW) pseudopotentials are adopted in all simulations. After geometry optimization at 0 K, 10-ps long AIMD trajectories under a certain temperature (e.g., T = 100 K) are obtained in the microcanonical ensemble, where the effects of thermal phonon excitation are included. The energies of KS orbitals and NAC are calculated along the AIMD trajectory with a time step of 1 fs. Then, the relaxation of photoexcited electrons is simulated based on the FSSH algorithm by randomly selecting 600 initial geometries from the initial 2 ps AIMD trajectory. Detailed calculation parameters are shown in Note S2.

ASSOCIATED CONTENT

Data Availability Statement

The data that support the plots within this paper and other findings of this study, and code and mathematical algorithms that support the findings of this study, are available from the corresponding authors upon reasonable request.

https://doi.org/10.1021/acs.jpclett.3c01685
J. Phys. Chem. Lett. 2023, 14, 8312−8319

Supporting Information

The Supporting Information is available free of charge at https://pubs.acs.org/doi/10.1021/acs.jpclett.3c01685.

Description of calculation methods and details. The influence of polaron configurations and temperature effects on photocarrier recombination. Phonon modes coupled to different electron transition channels (PDF)

AUTHOR INFORMATION

Corresponding Authors

Ying Jiang − *International Center for Quantum Materials, School of Physics and Interdisciplinary Institute of Light-Element Quantum Materials and Research Center for Light-Element Advanced Materials, Peking University, Beijing 100871, China;* orcid.org/0000-0002-6887-5503; Email: yjiang@pku.edu.cn

Sheng Meng − *Beijing National Laboratory for Condensed Matter Physics and Institute of Physics, Chinese Academy of Sciences, Beijing 100190, China; School of Physical Sciences, University of Chinese Academy of Sciences, Beijing 100049, China; Songshan Lake Materials Laboratory, Dongguan, Guangdong 523808, China;* orcid.org/0000-0002-1553-1432; Email: smeng@iphy.ac.cn

Authors

Huimin Wang − *Beijing National Laboratory for Condensed Matter Physics and Institute of Physics, Chinese Academy of Sciences, Beijing 100190, China; School of Physical Sciences, University of Chinese Academy of Sciences, Beijing 100049, China;* orcid.org/0000-0002-7096-2155

Huixia Fu − *Center of Quantum Materials and Devices, College of Physics, Chongqing University, Chongqing 401331, China*

Peiwei You − *Beijing National Laboratory for Condensed Matter Physics and Institute of Physics, Chinese Academy of Sciences, Beijing 100190, China; School of Physical Sciences, University of Chinese Academy of Sciences, Beijing 100049, China;* orcid.org/0000-0003-1606-4810

Cui Zhang − *Beijing National Laboratory for Condensed Matter Physics and Institute of Physics, Chinese Academy of Sciences, Beijing 100190, China; Songshan Lake Materials Laboratory, Dongguan, Guangdong 523808, China;* orcid.org/0000-0002-2154-5187

Complete contact information is available at: https://pubs.acs.org/10.1021/acs.jpclett.3c01685

Author Contributions

S.M. and Y.J. conceived, designed, and supervised the research. The calculations were performed by H.W., with help from H.F., P.Y., and C.Z. All authors contributed to the analysis and discussion of the data. H.W. and S.M. wrote the manuscript.

Notes

The authors declare no competing financial interest.

ACKNOWLEDGMENTS

We acknowledge partial financial support from the National Key Research and Development Program of China (Nos. 2021YFA1400503 and 2021YFA1400201), National Natural Science Foundation of China (No. 11934003, No. 12025407, No. 11974400), and Chinese Academy of Sciences (No. YSBR-047 and No. XDB330301).

REFERENCES

(1) Pastor, E.; Sachs, M.; Selim, S.; Durrant, J. R.; Bakulin, A. A.; Walsh, A. Electronic defects in metal oxide photocatalysts. *Nat. Rev. Mater.* **2022**, *7* (7), 503−521.

(2) Franchini, C.; Reticcioli, M.; Setvin, M.; Diebold, U. Polarons in materials. *Nat. Rev. Mater.* **2021**, *6* (7), 560−586.

(3) Emin, D. *Polarons*; Cambridge University Press, 2013.

(4) Zhang, S.; Wei, T.; Guan, J.; Zhu, Q.; Qin, W.; Wang, W.; Zhang, J.; Plummer, E. W.; Zhu, X.; Zhang, Z.; et al. Enhanced superconducting state in FeSe/$SrTiO_3$ by a dynamic interfacial polaron mechanism. *Phys. Rev. Lett.* **2019**, *122* (6), 066802.

(5) Emin, D.; Hillery, M. S. Formation of a large singlet bipolaron: Application to high-temperature bipolaronic superconductivity. *Phys. Rev. B Condens Matter* **1989**, *39* (10), 6575−6593.

(6) Emin, D. Formation, motion, and high-temperature superconductivity of large bipolarons. *Phys. Rev. Lett.* **1989**, *62* (13), 1544−1547.

(7) Morita, K.; Kumagai, Y.; Oba, F.; Walsh, A. Switchable electric dipole from polaron localization in dielectric crystals. *Phys. Rev. Lett.* **2022**, *129* (1), 017601.

(8) Selcuk, S.; Selloni, A. Facet-dependent trapping and dynamics of excess electrons at anatase TiO_2 surfaces and aqueous interfaces. *Nat. Mater.* **2016**, *15* (10), 1107−1112.

(9) Diebold, U. The surface science of titanium dioxide. *Surf. Sci. Rep.* **2003**, *48*, 53−229.

(10) Zuo, F.; Wang, L.; Wu, T.; Zhang, Z.; Borchardt, D.; Feng, P. Self-doped Ti^{3+} enhanced photocatalyst for hydrogen production under visible light. *J. Am. Chem. Soc.* **2010**, *132*, 11856−11857.

(11) Setvin, M.; Franchini, C.; Hao, X.; Schmid, M.; Janotti, A.; Kaltak, M.; Van de Walle, C. G.; Kresse, G.; Diebold, U. Direct view at excess electrons in TiO_2 rutile and anatase. *Phys. Rev. Lett.* **2014**, *113* (8), 086402.

(12) Di Valentin, C.; Pacchioni, G.; Selloni, A. Electronic structure of defect states in hydroxylated and reduced rutile TiO_2 (110) surfaces. *Phys. Rev. Lett.* **2006**, *97* (16), 166803.

(13) Wang, Z.; Wen, B.; Hao, Q.; Liu, L. M.; Zhou, C.; Mao, X.; Lang, X.; Yin, W. J.; Dai, D.; Selloni, A.; et al. Localized excitation of Ti^{3+} ions in the photoabsorption and photocatalytic activity of reduced rutile TiO_2. *J. Am. Chem. Soc.* **2015**, *137* (28), 9146−9152.

(14) Reticcioli, M.; Sokolovic, I.; Schmid, M.; Diebold, U.; Setvin, M.; Franchini, C. Interplay between adsorbates and polarons: CO on rutile TiO_2 (110). *Phys. Rev. Lett.* **2019**, *122* (1), 016805.

(15) Cheng, C.; Zhu, Y.; Fang, W. H.; Long, R.; Prezhdo, O. V. CO adsorbate promotes polaron photoactivity on the reduced rutile TiO_2(110) surface. *JACS Au* **2022**, *2* (1), 234−245.

(16) Reticcioli, M.; Setvin, M.; Hao, X.; Flauger, P.; Kresse, G.; Schmid, M.; Diebold, U.; Franchini, C. Polaron-driven surface reconstructions. *Phys. Rev. X* **2017**, *7*, 031053, DOI: 10.1103/PhysRevX.7.031053.

(17) Yim, C. M.; Watkins, M. B.; Wolf, M. J.; Pang, C. L.; Hermansson, K.; Thornton, G. Engineering polarons at a metal oxide surface. *Phys. Rev. Lett.* **2016**, *117* (11), 116402.

(18) Zhang, D.; Han, Z. K.; Murgida, G. E.; Ganduglia-Pirovano, M. V.; Gao, Y. Oxygen-vacancy dynamics and entanglement with polaron hopping at the reduced CeO_2 (111) surface. *Phys. Rev. Lett.* **2019**, *122* (9), 096101.

(19) Reticcioli, M.; Setvin, M.; Schmid, M.; Diebold, U.; Franchini, C. Formation and dynamics of small polarons on the rutile TiO_2(110) surface. *Phys. Rev. B* **2018**, *98*, 045306 DOI: 10.1103/PhysRevB.98.045306.

(20) Gao, C.; Zhang, L.; Zheng, Q.; Zhao, J. Tuning the lifetime of photoexcited small polarons on rutile TiO2 surface via molecular adsorption. *J. Phys. Chem. C* **2021**, *125* (49), 27275−27282.

(21) Guo, C.; Meng, X.; Fu, H.; Wang, Q.; Wang, H.; Tian, Y.; Peng, J.; Ma, R.; Weng, Y.; Meng, S.; et al. Probing nonequilibrium dynamics of photoexcited polarons on a metal-oxide surface with atomic precision. *Phys. Rev. Lett.* **2020**, *124* (20), 206801.

(22) Shockley, W.; Read, W. T. Statistics of the recombinations of holes and electrons. *Phys. Rev.* **1952**, *87* (5), 835−842.

(23) Papageorgiou, A. C.; Beglitis, N. S.; Pang, C. L.; Teobaldi, G.; Cabailh, G.; Chen, Q.; Fisher, A. J.; Hofer, W. A.; Thornton, G. Electron traps and their effect on the surface chemistry of TiO_2 (110). *Proc. Natl. Acad. Sci.* **2010**, *107* (6), 2391−2396.
(24) Bikondoa, O.; Pang, C. L.; Ithnin, R.; Muryn, C. A.; Onishi, H.; Thornton, G. Direct visualization of defect-mediated dissociation of water on TiO2(110). *Nat. Mater.* **2006**, *5* (3), 189−192.
(25) Lee, J.; Sorescu, D. C.; Deng, X. Electron-induced dissociation of CO_2 on TiO_2 (110). *J. Am. Chem. Soc.* **2011**, *133* (26), 10066−10069.
(26) Schaub, R.; Thostrup, P.; Lopez, N.; Laegsgaard, E.; Stensgaard, I.; Norskov, J. K.; Besenbacher, F. Oxygen vacancies as active sites for water dissociation on rutile TiO_2 (110). *Phys. Rev. Lett.* **2001**, *87* (26), 266104.
(27) Hirakawa, H.; Hashimoto, M.; Shiraishi, Y.; Hirai, T. Photocatalytic conversion of nitrogen to ammonia with water on surface oxygen vacancies of titanium dioxide. *J. Am. Chem. Soc.* **2017**, *139* (31), 10929−10936.
(28) Zhang, L.; Chu, W.; Zheng, Q.; Zhao, J. Effects of oxygen vacancies on the photoexcited carrier lifetime in rutile TiO2. *Phys. Chem. Chem. Phys.* **2022**, *24*, 4743.
(29) Ozawa, K.; Yamamoto, S.; Yukawa, R.; Liu, R.; Emori, M.; Inoue, K.; Higuchi, T.; Sakama, H.; Mase, K.; Matsuda, I. What determines the lifetime of photoexcited carriers on TiO_2 surfaces? *J. Phys. Chem. C* **2016**, *120* (51), 29283−29289.
(30) Corby, S.; Francas, L.; Kafizas, A.; Durrant, J. R. Determining the role of oxygen vacancies in the photoelectrocatalytic performance of WO_3 for water oxidation. *Chem. Sci.* **2020**, *11* (11), 2907−2914.
(31) Das, B.; Aguilera, I.; Rau, U.; Kirchartz, T. What is a deep defect? Combining Shockley-Read-Hall statistics with multiphonon recombination theory. *Phys. Rev. Mater.* **2020**, *4*, 024602, DOI: 10.1103/PhysRevMaterials.4.024602.
(32) Zhang, C.; Shi, Y.; Si, Y.; Liu, M.; Guo, L.; Zhao, J.; Prezhdo, O. V. Improved carrier lifetime in $BiVO_4$ by spin protection. *Nano Lett.* **2022**, *22* (15), 6334−6341.
(33) Chu, W.; Zheng, Q.; Prezhdo, O. V.; Zhao, J.; Saidi, W. A. Low-frequency lattice phonons in halide perovskites explain high defect tolerance toward electron-hole recombination. *Sci. Adv.* **2020**, *6* (7), eaaw7453, DOI: 10.1126/sciadv.aaw7453
(34) Zhang, L.; Chu, W.; Zheng, Q.; Benderskii, A. V.; Prezhdo, O. V.; Zhao, J. Suppression of electron-hole recombination by intrinsic defects in 2D monoelemental material. *J. Phys. Chem. Lett.* **2019**, *10* (20), 6151−6158.
(35) Li, J.; Yuan, Z.-K.; Chen, S.; Gong, X.-G.; Wei, S.-H. Effective and noneffective recombination center defects in Cu_2ZnSnS_4: Significant difference in carrier capture cross sections. *Chem. Mater.* **2019**, *31* (3), 826−833.
(36) Kim, S.; Park, J.-S.; Walsh, A. Identification of killer defects in kesterite thin-film solar cells. *ACS Energy Letters* **2018**, *3* (2), 496−500.
(37) Tully, J. C.; Preston, R. K. Trajectory surface hopping approach to nonadiabatic molecular collisions: The reaction of H^+ with D_2. *J. Chem. Phys.* **1971**, *55* (2), 562−572.
(38) Barbatti, M. Nonadiabatic dynamics with trajectory surface hopping method. *Wiley Interdisciplinary Reviews: Computational Molecular Science* **2011**, *1* (4), 620−633.
(39) Kowalski, P. M.; Camellone, M. F.; Nair, N. N.; Meyer, B.; Marx, D. Charge localization dynamics induced by oxygen vacancies on the TiO_2 (110) surface. *Phys. Rev. Lett.* **2010**, *105* (14), 146405.
(40) Deskins, N. A.; Rousseau, R.; Dupuis, M. Distribution of Ti^{3+} surface sites in reduced TiO_2. *J. Phys. Chem. C* **2011**, *115* (15), 7562−7572.
(41) Deskins, N. A.; Dupuis, M. Electron transport via polaron hopping in bulk TiO_2: A density functional theory characterization. *Phys. Rev. B* **2007**, *75* (19), 195212.
(42) Ozawa, K.; Emori, M.; Yamamoto, S.; Yukawa, R.; Yamamoto, S.; Hobara, R.; Fujikawa, K.; Sakama, H.; Matsuda, I. Electron-hole recombination time at TiO_2 single-crystal surfaces: Influence of surface band bending. *J. Phys. Chem. Lett.* **2014**, *5* (11), 1953−1957.
(43) Boch, J.; Saigne, F.; Dusseau, L.; Schrimpf, R. D. Temperature effect on geminate recombination. *Appl. Phys. Lett.* **2006**, *89* (4), DOI: 10.1063/1.2236707.
(44) Kruger, P.; Bourgeois, S.; Domenichini, B.; Magnan, H.; Chandesris, D.; Le Fevre, P.; Flank, A. M.; Jupille, J.; Floreano, L.; Cossaro, A.; et al. Defect states at the TiO_2(110) surface probed by resonant photoelectron diffraction. *Phys. Rev. Lett.* **2008**, *100* (5), 055501.
(45) Carneiro, L. M.; Cushing, S. K.; Liu, C.; Su, Y.; Yang, P.; Alivisatos, A. P.; Leone, S. R. Excitation-wavelength-dependent small polaron trapping of photoexcited carriers in alpha-Fe_2O_3. *Nat. Mater.* **2017**, *16* (8), 819−825.
(46) Craig, C. F.; Duncan, W. R.; Prezhdo, O. V. Trajectory surface hopping in the time-dependent Kohn-Sham approach for electron-nuclear dynamics. *Phys. Rev. Lett.* **2005**, *95* (16), 163001.
(47) Kresse, G.; Furthmüller, J. Efficient iterative schemes for ab initio total-energy calculations using a plane-wave basis set. *Phys. Rev. B* **1996**, *54* (16), 11169.
(48) Perdew, J. P.; Burke, K.; Ernzerhof, M. Generalized gradient approximation made simple. *Phys. Rev. Lett.* **1996**, *77* (18), 3865−3868.
(49) Perdew, J. P.; Ruzsinszky, A.; Csonka, G. I.; Vydrov, O. A.; Scuseria, G. E.; Constantin, L. A.; Zhou, X.; Burke, K. Restoring the density-gradient expansion for exchange in solids and surfaces. *Phys. Rev. Lett.* **2008**, *100* (13), 136406.

https://doi.org/10.1021/acs.jpclett.3c01685
J. Phys. Chem. Lett. 2023, 14, 8312−8319